Available online at www.sciencedirect.com
SCIENCE DIRECT®
PHOTONICS AND NANOSTRUCTURES Fundamentals and Applications
Photonics and Nanostructures – Fundamentals and Applications 1 (2003) 1–13
www.elsevier.com/locate/photonics

Review

Silicon-based two-dimensional photonic crystal waveguides

C. Jamois [a,*], R.B. Wehrspohn [a,b], L.C. Andreani [c], C. Hermann [d], O. Hess [d,e], U. Gösele [a]

[a] *Max-Planck Institut für Mikrostrukturphysik, Weinberg 2, 06120 Halle, Germany*
[b] *Nanophotonic Materials Group, Department of Physics, University of Paderborn, Paderborn, Germany*
[c] *INFM and Dipartimento di Fisica A. Volta, Università di Pavia, Via Bassi 6, 27100 Pavia, Italy*
[d] *DLR Stuttgart, Institut für Technische Physik, Theoretische Quantenelektronik, Pfaffenwaldring 38-40, 70569 Stuttgart, Germany*
[e] *Advanced Technology Institute, School of Electronics and Physical Sciences, University of Surrey, Guildford, Surrey GU2 7XH, UK*

Received 14 July 2003; received in revised form 8 October 2003; accepted 10 October 2003

Abstract

A review of the properties of silicon-based two-dimensional (2D) photonic crystals is given, essentially infinite 2D photonic crystals made from macroporous silicon and photonic crystal slabs based on silicon-on-insulator basis. We discuss the bulk photonic crystal properties with particular attention to the light cone and its impact on the band structure. The application for wave guiding is discussed for both material systems, and compared to classical waveguides based on index-guiding. Losses of resonant waveguide modes above the light line are discussed in detail.

Keywords: Silicon; Photonic crystal; Waveguides

1. Introduction

In the last decades strong effort has been carried out to investigate and control the optical properties of materials, to confine light in specified areas, to prohibit its propagation or to allow it to propagate only in certain directions and at certain frequencies. The introduction of components based on total internal reflection for light guidance, such as optical fibers or integrated ridge waveguides, has already enabled a revolution in the telecommunication and optical industry. In parallel to that, another way of controlling light based on Bragg diffraction has already been used in many devices like dielectric mirrors. In 1987, the principle of dielectric mirrors leading to one-dimensional (1D) light reflection was generalized to two and three dimensions [1,2] founding a new class of materials: photonic crystals. Since then, this new field has gained continuously increasing interest [3]. Photonic crystals are materials with a periodic dielectric constant. If the wavelength of light incident on the crystal is of the same order of magnitude as the periodicity, the multiple-scattered waves at the dielectric interfaces interfere, leading to a band structure for photons. If the difference between the dielectric constants of the materials composing the photonic crystal is high enough, a photonic band gap—i.e. a forbidden frequency range in a certain direction for a certain polarization—can

* Corresponding author. Tel.: +49-345-55-82-903; fax: +49-345-55-11-223.
E-mail address: jamois@mpi-halle.de (C. Jamois).

1569-4410/$ – see front matter © 2003 Elsevier B.V. All rights reserved.
doi:10.1016/j.photonics.2003.10.001

occur. However, a complete photonic band gap—i.e. a forbidden frequency range in all directions for all polarizations—can occur only in three-dimensional (3D) photonic crystals. Although these 3D photonic crystals look very promising and have been theoretically widely studied, their experimental fabrication is still a challenge [4–8]. Therefore, 2D photonic crystals, which are much easier to fabricate and which still offer most of the interesting properties of their 3D counterparts, have been investigated intensively. In the ideal case, 2D photonic crystals are infinitely-extended structures with a dielectric constant which is periodic in a plane and homogeneous in the third dimension. However, experimental structures are always finite, leading to scattering losses in the third dimension [9]. More recently the concept of photonic crystal slabs consisting of a thin 2D photonic crystal surrounded by a lower-index material has emerged and is now widely studied, because it offers a compromise between 2D and 3D concepts. Indeed, combining the index-guiding in the vertical direction with the presence of the photonic crystal in the plane of periodicity a 3D control of light can be achieved [10–12]. Among the several interesting effects in photonic crystals that can be used for a multitude of applications, such as modification of spontaneous emission [13,14] or effects based on the particular dispersion properties like birefringence [15], superprism effect and negative refraction [16–19], one of the important effects relies on the existence of the band gap for wave guiding purposes. In this paper, some properties of 2D photonic crystals are studied, assuming first an infinite height (Section 2) and then a finite one (Section 3). Subsequently, the influence of introducing a line defect into the photonic crystal lattice to built a waveguide is discussed, first in the case of infinite 2D photonic crystals (Section 4) and finally in photonic crystal slabs (Section 5).

2. Infinite 2D photonic crystals

Typically, 2D photonic crystals consist of a lattice of parallel rods embedded in a substrate of different dielectric constant. This can be either air pores in a dielectric or dielectric rods in air ordered in a square or hexagonal lattice, such that the dielectric constant is homogeneous in the direction parallel to the rod axis—generally defined as z-direction—and periodic in the (x, y)-plane:

$$\varepsilon(\vec{r}) = \varepsilon(\vec{r} + \vec{r}) \tag{1}$$

where $\vec{r}$ is any linear combination of the two unit vectors $\vec{a}_1$ and $\vec{a}_2$ of the 2D photonic crystal lattice:

$$\vec{r} = l\vec{a}_1 + m\vec{a}_2 \tag{2}$$

Due to the periodicity, the eigenfunctions of the system can be written in the form of Bloch states, in analogy to solid state physics. In the case that the magnetic field $\vec{H}$ is used as the variable this reads:

$$\vec{H}_{n,\vec{k}}(\vec{r}) = \mathrm{e}^{\mathrm{i}\vec{k}\cdot\vec{r}} \cdot \vec{u}_{n,\vec{k}}(\vec{r}) \tag{3}$$

where n is the frequency band index, $\vec{k}$ the wave vector, and the function $\vec{u}_{n,\vec{k}}$ has the periodicity of the photonic crystal:

$$\vec{u}_{n,\vec{k}}(\vec{r}) = \vec{u}_{n,\vec{k}}(\vec{r} + \vec{r}) \tag{4}$$

If the materials constituting the photonic crystal are assumed to be linear, isotropic, non-magnetic and free of charges, the following wave equation is obtained by combining Maxwell's equations:

$$\vec{\nabla} \times \left(\frac{1}{\varepsilon(\vec{r})} \vec{\nabla} \times \vec{H}(\vec{r}) \right) = \frac{\omega^2}{c^2} \vec{H}(\vec{r}) \tag{5}$$

with

$$\vec{\nabla} \cdot \vec{H}(\vec{r}) = 0 \tag{6}$$

This is an eigenvalue problem where the eigenvectors $\vec{H}(\vec{r})$ are called harmonic modes, and the eigenvalues $(\omega/c)^2$ are proportional to the squared frequency of these modes, c being the speed of light.

By solving the master Eq. (5) for k-vectors along the irreducible Brillouin zone of the photonic crystal, the band structure of the photonic crystal is obtained. Because the (x, y)-plane of periodicity of the 2D photonic crystal is a mirror plane of the system, the polarizations decouple, i.e. the modes can be separated into transverse-electric (TE) modes having only H_z, E_x and E_y as non-zero components, and transverse-magnetic (TM) modes with the only non-zero components E_z, H_x and H_y. Since TE (resp. TM) modes have their magnetic (resp. electric) field oriented along the pore axis, they are often also called H (resp. E) modes. The band structures for TE and TM polarizations are usually completely different, because the electric field (resp. magnetic field) for TE and TM polarizations is

oriented in different directions relatively to the dielectric interfaces within the photonic crystal. In particular, band gaps can exist for one polarization and not for the other, or the position of the band gaps can be very different. It has turned out that, while for systems consisting of dielectric cylinders in air a complete band gap, i.e. a band gap for both polarizations, can be obtained only in a honeycomb lattice, the hexagonal lattice of air holes in dielectric opens up a complete 2D photonic band gap for a dielectric contrast n_2/n_1 larger than 2.6 [3,20].

Fig. 1 gives an example of a band structure in the case of a hexagonal lattice of air pores in silicon with a relative radius r/a of 0.43, where a is the lattice constant of the photonic crystal. The band structure calculation was performed using the MIT package, a block-iterative frequency-domain code [21] with a grid of 64 points per lattice constant yielding good convergence of the results. For this relative radius value, a large TE band gap exists from 0.275 to 0.460 in normalized frequency $\omega a/2\pi c$ and a smaller TM band gap from 0.385 to 0.405 that overlaps with the TE band gap, leading to a complete 2D band gap in this frequency range. The variation of the photonic band gap position with relative pore radius—the so-called gap map—for a hexagonal lattice of air pores in silicon is shown in Fig. 2. In this system, the complete band gap exists only for a relative radius larger than 0.4, the largest gap–midgap ratio—ratio between band gap width and midgap frequency—being 16.3% for a pore radius $r/a = 0.478$. However, such very large relative radius values are quite difficult to achieve experimentally. Therefore, most of the work based on the existence of a band gap in 2D photonic crystals has focussed on the TE band gap only, which is still quite large for smaller radii, e.g. at $r/a = 0.366$ the gap–midgap ratio for TE modes is as large as 42.5%.

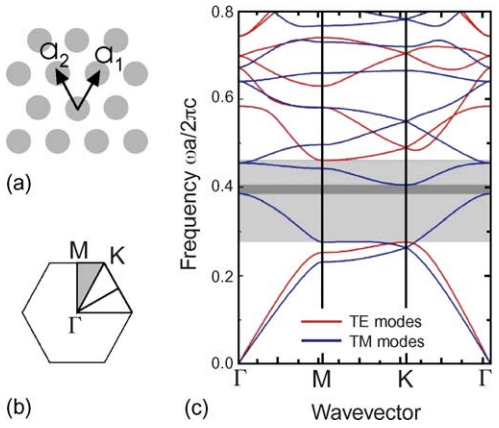

Fig. 1. (a) 2D hexagonal lattice and (b) its first Brillouin zone with the irreducible Brillouin zone delimited by the three high-symmetry points Γ, M and K. (c) Band structure for a hexagonal array of air pores in silicon ($\varepsilon = 11.6$, $r/a = 0.43$) along the k-path Γ–M–K–Γ for TE (red lines) and TM (blue lines) polarizations. The light grey region highlights the TE band gap and the dark grey region the TM (resp. complete) band gap (MIT package calculation).

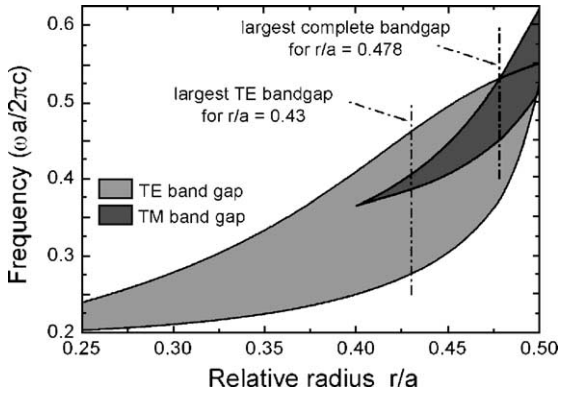

Fig. 2. 2D gap map (normalized frequency $\omega a/2\pi c$ vs. relative pore radius r/a) for a hexagonal lattice of air holes in silicon ($\varepsilon = 11.6$). The position of the largest gap-midgap ratio is indicated (MIT package calculation).

From an experimental point of view, the approximation of infinitely long pores or rods can be applied only in structures exhibiting high aspect ratios (ratio between pore/rod length to pore/rod diameter). We have already verified [22] that aspect ratios larger than 20 are necessary for the band structures of finite-height silicon-based 2D photonic crystals obtained by 2D numerical simulations to overlap perfectly with full 3D ones. This is difficult to achieve with conventional dry etching techniques. However, a good candidate for experimental study of 2D photonic crystals is macroporous silicon, consisting of a periodic array of air pores in silicon. Indeed, in these structures prepared by photo-electrochemical dissolution of silicon in hydrofluoric acid [23,24], very high aspect ratios up to 500 can be obtained, as illustrated in Fig. 3. It has been recently shown that the optical properties of macroporous silicon can be well described by 2D simulations [25,26].

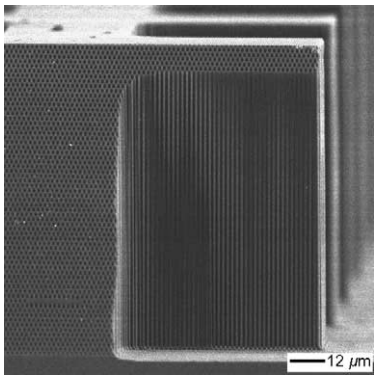

Fig. 3. SEM image of a two-dimensional hexagonal lattice of air pores in silicon with a lattice constant of 1.5 μm. The pore depth is around 100 μm. The bevelled etched part in front reveals the high uniformity of the structure from the top down to the bottom of the pores (courtesy of A. Birner, MPI Halle).

Fig. 4a shows the reflectivity of TE-polarized light incident on a photonic crystal consisting of macroporous silicon in the Γ–M direction. The photonic crystal has a hexagonal lattice of air pores with a relative radius r/a of 0.366, and a lattice constant of 700 nm. The reflection was measured using a Fourier transformation infrared spectrometer (FTIR) with attached optical IR microscope and calcium fluoride beam splitter covering a spectral region from UV to mid IR. The light source was a broadband tungsten lamp. The band structure of the photonic crystal is presented in Fig. 4b. However, these curves cannot be compared directly with the band structure, because not all the bands yield very high transmission. Indeed, for the main directions Γ–M and Γ–K the plane defined by the wave vector and the pore axis is a mirror plane of the crystal. Thus, the modes can be separated into laterally even modes or odd modes. Since always the $E_{\parallel}$- or $H_{\perp}$-field components have to be considered to define the mode symmetry, laterally even (odd) symmetry corresponds to laterally odd (even) H_z-field distribution. The lateral symmetry of the modes is illustrated in Fig. 5, taking as examples the H_z-field distribution of the first and fourth bands at the M-point. While coupling from an incident plane-wave into the photonic crystal, only the odd modes are excited. Therefore, the zero-transmission (resp. high reflectivity) regions do not correspond only to band gaps, but to frequency regions where no laterally odd mode exists. Thus, the agreement between the measured transmission and the calculated band structure is very good.

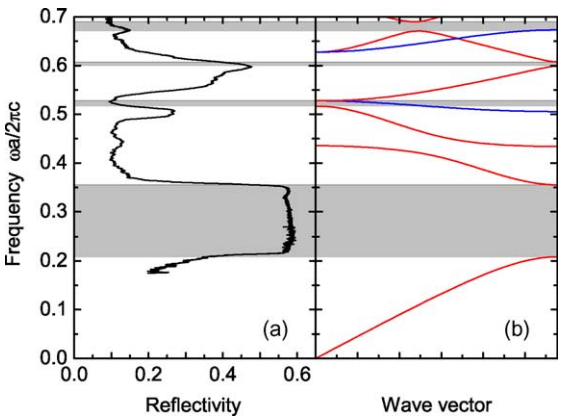

Fig. 4. (a) Reflectivity of TE-polarized light incident onto a 2D photonic crystal made of a hexagonal lattice of air pores in silicon with a relative radius r/a of 0.366 and a lattice constant of 700 nm. The light beam is parallel to the plane of periodicity of the crystal in the Γ–M direction (courtesy of S. Schweizer (sample) and S. Richter (measurement), MPI Halle). (b) Corresponding band structure for TE-polarization (MIT package calculation). The modes are sorted as laterally even (blue) or laterally odd (red) modes. The regions where no odd mode exists are highlighted in grey and correspond to the high-reflectivity regions.

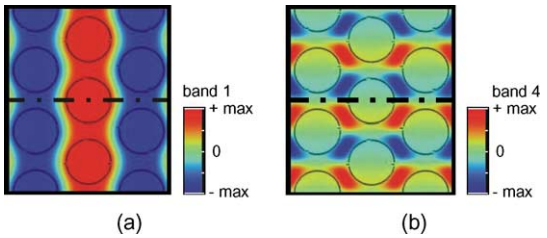

Fig. 5. H_z-field distribution of the (a) first and (b) fourth TE bands at the M-point for a 2D photonic crystal consisting of a hexagonal array of air pores in silicon with $r/a = 0.366$ (MIT package calculation). If we consider the mirror plane defined by the Γ-M direction and the direction of the pore axis (dashed line) the first band has an odd symmetry and the fourth band an even one.

3. Photonic crystals slabs

Since 2D photonic crystals cannot, by definition, provide light confinement in the direction parallel to the pore axis, a way to avoid out-of-plane losses is the use of photonic crystal slabs. Slab structures consist

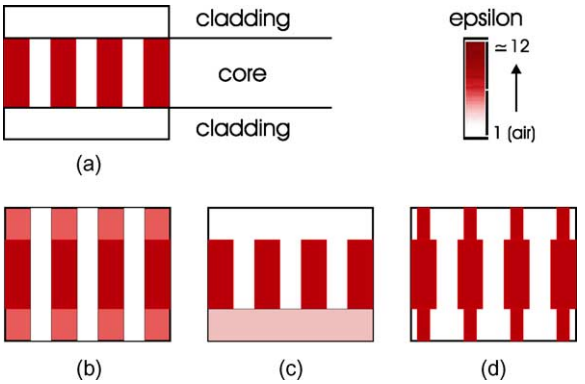

Fig. 6. Four examples of photonic crystal slabs (side view): (a) air-bridge structure with high index contrast between core and cladding, e.g. Si membrane, (b) low-index contrast heterostructure (e.g. AlGaAs/GaAs/AlGaAs system), (c) asymmetrical structure with two different claddings, the upper one usually being air, current in SOI-based photonic crystal slabs, and (d) modulated-pores structure achieved, e.g. in macroporous silicon.

of a thin 2D photonic crystal (core) surrounded by two layers of lower effective refractive index (claddings) that provide an index guiding by total internal reflection in the direction normal to the plane of the crystal, as in a planar waveguide. Different examples of photonic crystal slabs are shown in Fig. 6. The first one, the so-called "air-bridge" structure has been already largely studied [27,28]. It consists of a thin 2D photonic crystal in a high-index membrane surrounded by air (Fig. 6a). In this case, the index contrast between core and cladding is very high and light is strongly confined within the core. However, this type of structure is not easily integrable into a chip. The second example (Fig. 6b) is a photonic crystal slab made in a heterostructure, usually consisting of III–V semiconductor materials. In this case, the index-contrast between core and cladding is low, thus the mode profiles are quite extended, and the pores penetrate deeply into the cladding layers [29,30]. The third type of structure (Fig. 6c) is a hybrid case often found in SOI-based systems [28,31,32]. The lower cladding usually consists of an oxide layer, not necessarily structured, while in most cases the upper cladding consists only of air. Although this photonic crystal is easier to integrate into a chip than a membrane, the asymmetry of the mode profile within the structure leads to additional losses. In the case of a structured oxide layer, the effective refractive index in the cladding is close to 1, thus, the structure offers both advantages of being easily integrable and almost symmetrical. The ideal case would be a structure with two structured oxide claddings, leading to integrability, high light confinement and perfectly symmetrical mode profiles at the same time. Furthermore, unlike case (b), the presence of two structured claddings with low index should lead to low scattering losses from an experimental point of view. Indeed, even if the modes are theoretically guided and lossless, the experimental structures are never perfect and scattering losses occur due to irregularities, like roughness of the pore walls. These losses are expected to be smaller for structures with high vertical index contrast [33]. However, since high-aspect-ratio oxide structuring at a submicron scale is still a challenge, this type of system with two structured oxide claddings is very difficult to fabricate. These first three examples have in common that the effective index contrast between core and cladding is obtained by taking another material as in the slab to build the claddings. In the last case (Fig. 6d), the effective index contrast is obtained by modulation of the pore diameter, keeping the same material. In the cladding, the air filling fraction is higher, thus the effective refractive index is lower. This kind of structure can be obtained for example in macroporous silicon [22] and offers large freedom concerning the pore modulation and depth.

Because of the finite height of the photonic crystal slab, polarization mixing occurs and the modes are not purely TE (resp. TM)-polarized anymore. On the other hand, if the (x, y)-plane in the middle of the slab is a mirror plane of the structure, i.e., if both claddings are identical as in the examples shown in Fig. 6a, b and d, the modes can be separated into vertically even (with the H_z component having a symmetrical field distribution) and odd modes (antisymmetrical field distribution). However, the first-order modes, i.e. modes having no node in the vertical direction, have field distributions within the core that are very similar to the corresponding modes existing in infinite 2D photonic crystals. Furthermore, in the (x, y)-mirror plane itself, these modes are purely TE (resp. TM)-polarized [34]. Thus, for first-order modes the polarization mixing is quite small and the approximation even $\sim$ TE-polarized and odd $\sim$ TM-polarized can be assumed. Therefore, the terminologies TE (or H) modes and TM (or E) modes are found very often to refer to even and odd modes, respectively.

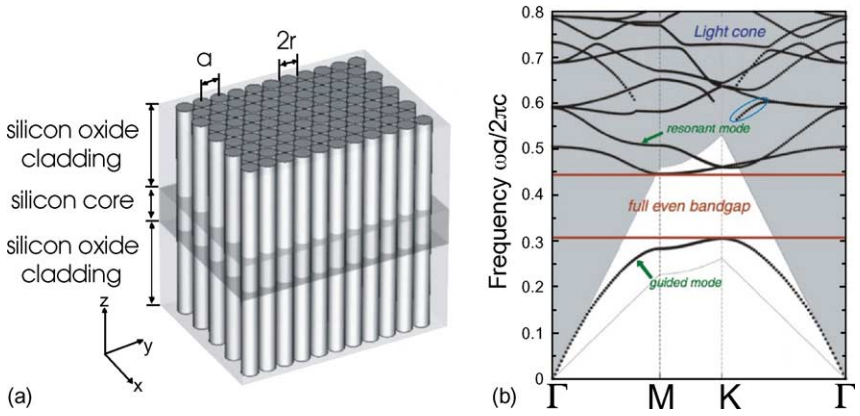

Fig. 7. (a) Photonic crystal slab consisting of a silicon core and two structured silicon oxide claddings (IOSOI structure) with air pores arranged in a hexagonal lattice. (b) Band structure of such a system having a relative thickness $h/a = 0.4$ and a relative radius of 0.366, even modes only. Above the light line of the cladding system (grey region) the modes are resonant, their lifetime can be very limited. Only below the light line (white region) the modes are guided and lossless. The position of the lowest second-order mode is highlighted in blue (2D plane-wave calculation taking as basis the eigenmodes of the corresponding planar waveguide [35]).

Beside the polarization mixing effect, another important difference between infinite 2D photonic crystals and photonic crystal slabs lies in the role of the light line, which is the lowest band in the cladding system. Indeed, the structure supports two kinds of modes (Fig. 7b) . If the slab thickness is not too small and the index contrast between core and cladding is not too low, there exist some states in the slab which form a photonic gap below the light line. The larger the index contrast between core and claddings, the more modes exist below the light line [10,35]. Since for this $(\vec{k}, \omega)$-set no state is allowed in the claddings, the modes of the slab are totally internally reflected at the interfaces between core and cladding and confined within the core. These modes are pure Bloch modes, they are lossless in the case of an ideal structure where no scattering occurs. Unlike symmetrical structures, in the case of asymmetrical structures the fundamental mode has a finite cutoff. The stronger the asymmetry, the higher the cutoff frequency of the mode, so that it may happen that the lowest mode lies entirely above the light line, and no guided mode exists at all [36]. Above the light line of the cladding material, the modes lie within the continuum of leaky modes of the planar waveguide. Therefore, they are resonant or “quasi-guided”, because they have intrinsic radiation losses related to out-of-plane diffraction. Their lifetime is varying, it can be very long (weak radiation losses) as well as very limited (strong radiation losses) [37]. A method to estimate the radiation losses a posteriori consists in including an effective loss into a 2D model through a dissipation mechanism, i.e. by inserting an imaginary index in the air holes and calculating the radiation losses using a first-order perturbation approximation. The value of the imaginary index is determined by fitting of the experimental data. This very efficient method has been first developed for a transfer-matrix code [9] and then been extended to a time-domain method [38].

A lot of theoretical work on photonic crystal slabs has focussed on guided modes only [10,11]. However, for practical applications, the modes above the light line must be considered too, because an incident wave can couple light to all the modes existing at a given frequency in a given direction, provided they have the proper symmetry. Due to the finite height of the structure, 3D calculations are necessary to determine the band structure. However, several 3D codes—like the MIT package—assume a periodicity in all three dimensions, which is not convenient for a photonic crystal slab. Due to the fictive periodicity in the vertical direction, some additional coupling between resonant modes occurs, which disturbs completely the band structure. Therefore, only guided modes can be calculated correctly, because they do not feel the fictive vertical periodicity. There are different methods to calculate resonant modes. A way is to use a 3D finite-difference time-domain (FDTD) code with open

boundary conditions on the top and the bottom of the structure [39,37]. It is also possible to perform 2D plane-wave calculations taking as a basis the eigenmodes of a planar waveguide where each layer has the same effective refractive index as the photonic crystal slab structure [35]. This is the method used in Fig. 7.

If the slab thickness is increased, the cutoff frequency of the higher-order modes decreases, exactly as in a planar waveguide. For too thick slabs, higher-order modes can exist within the first-order band gap of the photonic crystal slab. Thus, if these modes happen to have the right symmetry properties to be excited by an external light beam, they can limit the band gap or even destroy it completely. Reducing the vertical index contrast Δn, the cutoff frequency of the higher-order modes increases. A first guess to determine the cutoff frequency of the lowest second-order mode is to use the planar waveguide approximation. In this very simple approximation, we calculate the cutoff frequency of the second mode in a planar waveguide where each layer has the same effective refractive index as the photonic crystal slab, using the relation

$$\frac{h}{\lambda_0} = \frac{1}{2\sqrt{n_2^2 - n_1^2}} \tag{7}$$

where h is the thickness of the core, λ_0 the cutoff wavelength, n_1 and n_2 the effective indices in the claddings and in the core, respectively, and for a photonic crystal:

$$\frac{h}{\lambda_0} = \frac{h}{a}\frac{a}{\lambda_0} \tag{8}$$

with h/a the relative thickness of the slab and $a/\lambda_0 = \omega a/2\pi c$ the normalized cutoff frequency of the mode. There are different methods to determine the effective refractive index of a photonic crystal. We choose here to consider the light lines of the 2D systems corresponding to core and claddings and take the inverse of their tangent at the Γ-point. For example, for a photonic crystal slab consisting of a silicon slab ($\varepsilon = 11.6$) and two structured silicon oxide claddings ($\varepsilon = 2.1$) with a relative radius of 0.366, the effective refractive indices are 2.57 in the core and 1.25 in the claddings. This leads for a relative silicon thickness of 0.4 to a cutoff frequency of 0.56 for the first second-order mode. Such a system as well as the corresponding band structure have already been presented in Fig. 7. It can be seen on the band structure that the lowest second-order mode has a cutoff frequency around 0.57 that is very close to the value calculated using the planar waveguide approximation. Therefore, this very simple method gives already a good guess of the cutoff frequency of higher-order modes in photonic crystal slabs.

4. Waveguides in infinite 2D photonic crystals

If a line defect is introduced into the 2D photonic crystal lattice, e.g. by changing the pore radius of an entire pore line or removing it completely, some defect states are created. For a convenient design of the defect, some of these states ought to be located within the band gap of the photonic crystal. Since light can not propagate in the photonic crystal at this frequency, it is localized in the surrounding of the defect, i.e., the line defect acts as a waveguide. Fig. 8 shows some examples of linear waveguides in 2D photonic crystals.

The introduction of a line defect induces a symmetry breaking. Indeed, now the translation symmetry exists only in the direction parallel to the defect. Therefore, the new Brillouin zone is 1D, and the band structure of the 2D photonic crystal has to be projected onto the k-path Γ(0)–J(π/a) of the new Brillouin zone [40]. Fig. 9 shows the band structure for TE modes of a W1 waveguide consisting of a row of missing pores in the Γ–K direction, the photonic crystal consisting of a hexagonal lattice of air pores in silicon with relative radius 0.43. The band structure for the

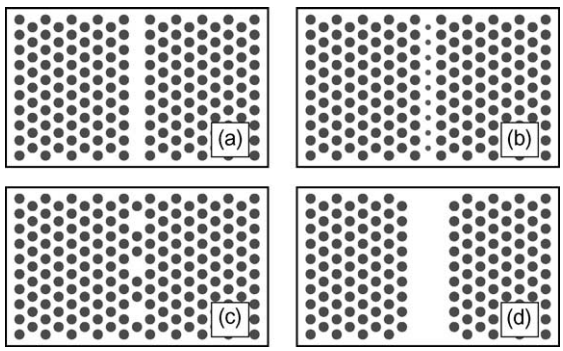

Fig. 8. Some examples of waveguides in 2D photonic crystals: (a) W1 waveguide (i.e. waveguide having a width of one pore row) consisting of a row of missing pores, (b) W1 waveguide consisting of a row of pores with smaller diameter, (c) coupled-cavity-waveguide and (d) W3 waveguide (i.e. three pore-rows wide).

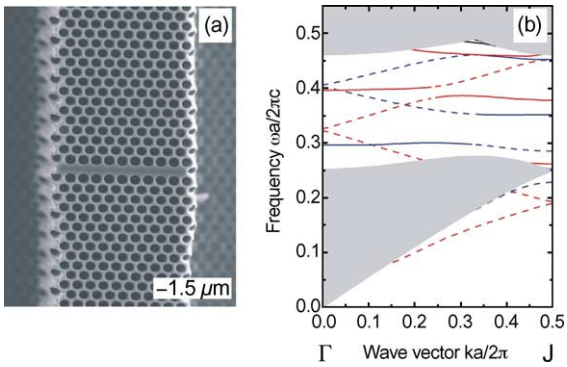

Fig. 9. (a) SEM picture and (b) band structure for the TE polarization of a linear waveguide in a 2D photonic crystal. The photonic crystal consists of a hexagonal lattice of air pores in silicon with lattice constant 1.5 μm and relative radius 0.43. The linear defect is made of a row of missing pores in the Γ–K direction. The defect modes are sorted into index-guided (dashed lines) and photonic-band-gap guided modes (solid lines) as well as into laterally odd (red lines) and even modes (blue lines) (MIT package calculation).

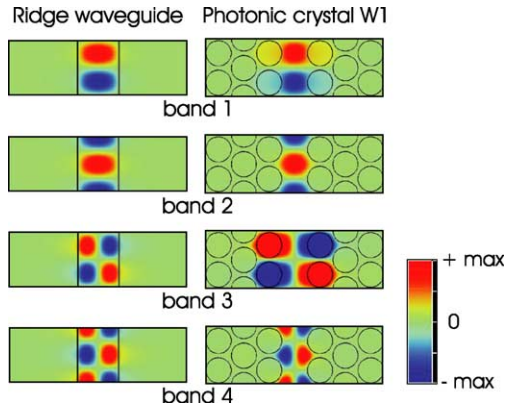

Fig. 10. Comparison between the H_z-field distributions of the four lowest index-guided modes in the photonic crystal waveguide presented in Fig. 9 (right) and in the corresponding ridge waveguide (left) having the same width and the same effective indices in the core (3.4 for silicon) and the claddings (1.55 for the system silicon/air pores with $r/a = 0.43$). The black lines on the left demarcate the silicon core of the ridge waveguide while the black circles on the right indicate the position of the air pores of the photonic crystal. (MIT package calculation).

corresponding bulk photonic crystal has already been presented in Fig. 1. The grey regions in Fig. 9 correspond to the continuum of projected bands of the bulk photonic crystal. Comparison with Fig. 1 shows that there is a TE band gap in the frequency region from 0.275 to 0.460 where several defect states are located. However, not all of these defect states are guided due to the presence of the photonic band gap. Indeed, in such a structure two guiding mechanisms coexist. The first one is based on the existence of the photonic band gap and the second one is classical index guiding due to the effective index contrast between the waveguide and its surrounding.

Since their existence is based on index contrast, index-guided modes (dashed lines) exist below the first band of the bulk photonic crystal. When they reach the J-point at the limit of the first Brillouin zone, they are folded back into the first Brillouin zone and continue to increase in direction of the Γ-point, and so on. Fig. 10 shows a comparison between the field distributions at the J-point of the two index-guided modes of Fig. 9 and those of the corresponding 2D ridge-waveguide having the same width and the same effective indices in core and cladding as the photonic crystal waveguide. There is good agreement between the fields of both systems, taking into account that the index-guided modes inside the photonic crystal waveguide are perturbed by the periodicity of the pores, which leads to the stop gap between the modes at the J-point. Considering first the two lowest-order modes (red dashed lines, having at the J-point the frequencies 0.190 and 0.193, respectively), it can be noticed that the first index-guided mode in the W1 waveguide extends more into the photonic crystal than the second one. This can be explained by the fact that the wavelength of the lowest mode is larger (the mode extension for fundamental modes is $\lambda/2$). The same phenomenon occurs in a much stronger way for the third and fourth bands, corresponding to the second-order mode in the ridge waveguide. These two bands (blue dashed lines) have the frequencies 0.228 and 0.285 at the J-point, respectively, band 3 lying below the region of bulk modes and band 4 within the band gap. We can explain the stronger energy gap between the two bands in the following way: in this case, the mode extension is λ, so that the mode profile of band 3 is large and has to extend into the surrounding photonic crystal. Thus, its field intensity is located partially in the air pores. Since the mode extension of band 4 is smaller, this mode can be very well located in the dielectric. Due to the important difference between the field distributions of these two second-order modes,

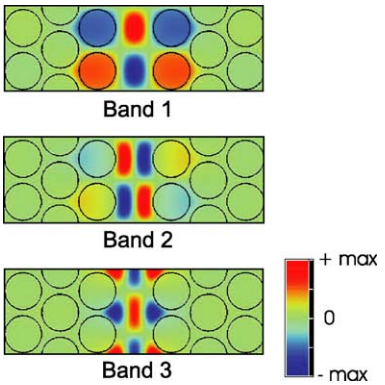

Fig. 11. H_z-field distributions of the three lowest photonic-band-gap-guided defect modes of the W1 waveguide presented in Fig. 9. The black circles indicate the position of the air pores of the photonic crystal. (MIT package calculation).

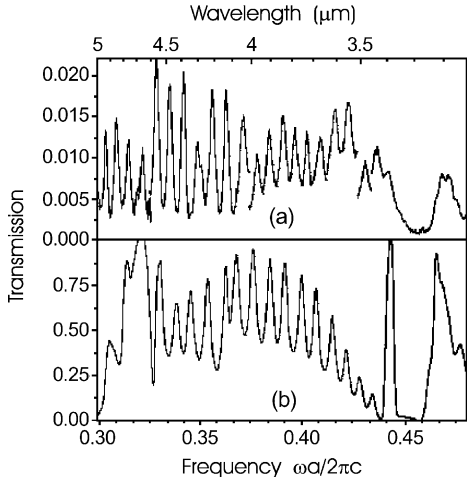

Fig. 12. (a) Transmission measurement and (b) FDTD calculation for the photonic crystal waveguide presented in Fig. 9. The waveguide is 18 lattice constants long. (reprinted from [42]).

a much larger energy gap is expected between them than between the two first ones. As a consequence, band 4 lies within the band gap of the photonic crystal.

Unlike the index-guided modes, the photonic-band-gap-guided modes exist only within the band gap of the photonic crystal (solid lines in Fig. 9). Their guiding mechanism is based on the absence of allowed states in the surrounding photonic crystal, and therefore presents a metallic-like behavior. Furthermore, contrary to index-guided modes, they exist also in waveguides where the core has a lower effective index as the surrounding photonic crystal [40]. Fig. 11 shows the field distributions of the three lowest photonic-band-gap-guided defect modes at the J-point, having frequencies 0.262, 0.352 and 0.378, respectively.

Another effect that can be noticed in Fig. 9 is anti-crossing. Indeed, only modes having different symmetries can cross each other without being disturbed. Modes having the same symmetry interact, leading to anti-crossing effects, as can be seen for the two laterally odd modes in the middle of the gap at a frequency around 0.39. The interaction between these two modes illustrates the fact that the distinction done between index- and band-gap guidance is not always a rigorous one. Moreover, it is possible to combine both, by inserting a slab waveguide in the middle of a photonic crystal [40,41].

Fig. 12 shows the transmission through a W1 waveguide consisting one row of missing pores in macroporous silicon, similar to that presented in Fig. 9. The line defect is 27 μm long (18 lattice constants). The transmission through the waveguide was measured with a pulsed laser source having a bandwidth of 200 nm and tunable over a large frequency range of the TE band gap ($3.1\,\mu m < \lambda < 5.5\,\mu m$) [26,42]. The measured spectrum in Fig. 12a exhibits pronounced Fabry–Perot resonances over a large spectral range which are caused by multiple reflections at the waveguide facets, and is in very good agreement with the corresponding 2D-FDTD transmission calculation of Fig. 12b. Again, as in the case of bulk photonic crystals, only the waveguide modes with laterally odd symmetry with respect to the mirror plane in the middle of the waveguide can be excited by the laser beam, so that the even modes do not contribute to the transmission.

Due to the photo-electrochemical fabrication process the diameter of the pores in the adjacent rows to the waveguide is increased, as can be seen in Fig. 9a. This leads to a shift of defect modes to higher frequencies. In the transmission calculation this feature has been taken into account. Therefore, if the reflection curves are compared with the band structure of Fig. 9, the small stopgap observed in the transmission curves for frequencies around 0.45 corresponds to the anti-crossing between odd modes in the middle of the band gap.

5. Waveguides in photonic crystal slabs

If a line defect is introduced into a photonic crystal slab lattice, the same phenomenon occurs as in the case of infinite 2D photonic crystals. For an appropriate design of the waveguide some defect states are located within the band gap of the photonic crystal, so that light is confined along the line defect in the plane of the crystal in this frequency range. Combining this in-plane confinement with the vertical confinement due to the index contrast in the vertical direction, a 3D light confinement is possible within a waveguide in a photonic crystal slab [27–31,40]. Fig. 13 shows the band structure of a W1 waveguide made of one row of missing pores in a photonic crystal slab, calculated using the MIT package. The photonic crystal consists of a silicon core with relative thickness 0.4 surrounded by two structured silicon oxide claddings (i.e., the air pores extend into the oxide claddings). The pores are arranged in a hexagonal lattice and have a relative radius of 0.366. The corresponding band structure for the bulk photonic crystal has been shown in Fig. 7. The lower grey region corresponds to the continuum of projected bulk bands, and the upper grey region to the light cone. The defect modes below the region of projected bulk modes are index-guided, as in the case of an infinite 2D photonic crystal. Furthermore, the field distributions (1–3) in the (x,y)-mirror plane in the middle of the silicon slab shown in Fig. 13 are very similar to the corresponding ones presented in Fig. 10. This is related to the fact that the defect modes are very well confined within the silicon core, as can be seen in the vertical cross sections shown in Fig. 13. Above the projected bulk modes, the defect modes lie within the band gap of the photonic crystal. They are vertically confined as long as they are in the white region below the light line. For in-plane confinement both guiding mechanism coexist as in the case of infinite 2D waveguide structures: either the modes are index-guided (like band 5) or they are guided due to the existence of the photonic band gap (like band 4). Again, comparison between the field distributions of these two defect modes and the two corresponding ones presented in Fig. 9a and band 4 in Fig. 10 show very strong similarities.

Above the light line the defect modes become resonant, i.e., they are still guided in the plane along the line defect but they are lossy in the vertical direction. Due to the intrinsic radiation losses, the light transmission through waveguides based on defect modes above

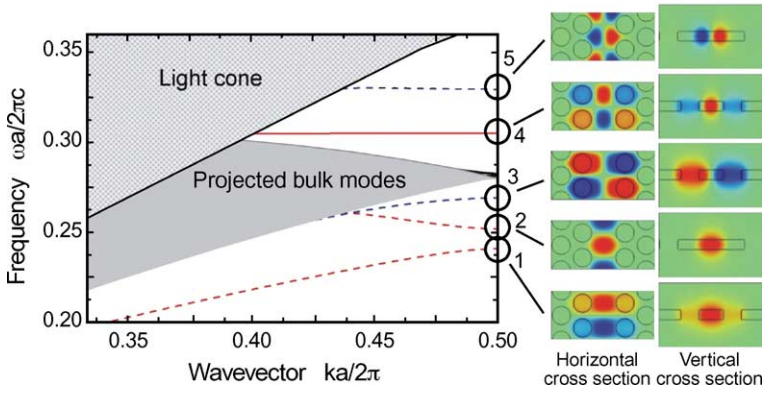

Fig. 13. Left: band structure of a W1 waveguide consisting of one row of missing pores in a photonic crystal slab. The photonic crystal is fabricated in a silicon core with relative thickness 0.4 surrounded by two structured silicon oxide claddings (MIT package calculation). The pores are arranged in a hexagonal lattice, and have a relative radius of 0.366. The lower grey region corresponds to the continuum of projected bulk bands, and the upper grey region to the light cone. The defect modes are sorted into index-guided (dashed lines) and photonic-band-gap guided modes (solid lines) as well as into laterally odd (red lines) and even modes (blue lines). Right: H_z-field distributions of the five defect modes which are guided at the boundary of the first Brillouin zone (J-point). The horizontal cross-sections show the field distributions in the (x, y)-mirror plane in the middle of the silicon slab, the black circles indicating the position of the pores. The vertical cross sections show the field distributions in the (x, z)-planes containing the intensity maxima, the black lines indicating the position of the silicon slab.

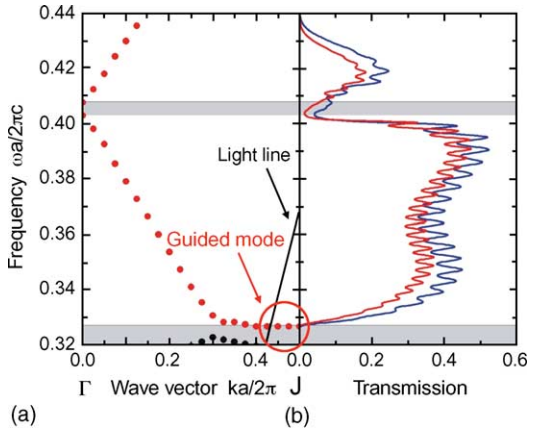

Fig. 14. (a) Band structure for odd modes of a photonic crystal waveguide having a relative silicon thickness of 0.3 and all other parameters like in Fig. 13 (3D FDTD calculation with open boundary conditions on the top and the bottom of the structure). Only the frequency range between 0.32 and 0.44 is shown, corresponding to the photonic band gap of the crystal. The grey regions correspond to the frequency regions within the photonic band gap where no defect mode exists. (b) Transmission through the waveguide with 30 (blue line) and 40 (red line) lattice constants length, respectively. The light is coupled in and out through a ridge waveguide having the same width and the same effective indices as the photonic crystal waveguide.

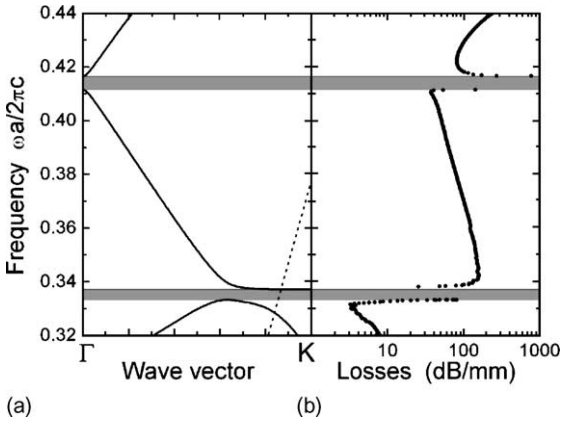

Fig. 15. (a) Band structure for odd modes of the same photonic crystal waveguide as in Fig. 14 and (b) corresponding intrinsic losses (2D plane-wave calculation [35,43]). The dashed line indicates the position of the light line. The small frequency shift observed while comparing with Fig. 14 comes from the fact that the two codes used converged towards slightly different values.

the light line can be quite low. Fig. 14a shows the band structure of a photonic crystal waveguide having a relative silicon thickness of 0.3, all the other parameters being the same as in Fig. 13. The corresponding transmission through this waveguide with 30a (resp. 40a) length is presented in Fig. 14b. The calculation takes into account light in- and out-coupling to the photonic crystal waveguide through a ridge waveguide having the same width and the same effective indices, leading to coupling losses of around 50%. The relative frequency range shown (0.32–0.44) corresponds to the photonic band gap of the crystal. Since laterally odd modes are of interest only the two odd defect bands are shown in the band structure, separated by a mini stop gap around 0.405. The light line of the cladding system is shown (black line). Thus, the first defect mode is guided only in the wave vector range 0.4–0.5, which corresponds to a very small frequency range. The main part of the lower defect band in Fig. 14 (for wave vectors below 0.4), contributing to the transmission, is resonant. From the difference in transmission between the two waveguide lengths the attenuation due to radiation losses is estimated to be in the order of 100 dB/mm for a lattice constant of 500 nm. This estimation is in good agreement with theoretical predictions [43] as well as experimental measurements on W1 waveguides in silicon [44]. Fig. 15 shows the conformity between the band structure and the intrinsic losses within the photonic crystal waveguide. It can be recognized that the losses of the lowest defect mode are in the order of 100 dB/mm on average, as predicted from the transmission calculation. When the wave vector increases towards the J point, the band crosses the light line and becomes guided. As expected, this corresponds to a very fast decrease of the losses. Above the light line, at the other band edge, while reaching the mini-stop gap at the Γ-point the slowing down of the group velocity leads to a large increase of the radiation losses. The same phenomena is observed at the lower limit of the band gap for frequencies around 0.335. The upper odd defect mode is entirely resonant, the corresponding low transmission presented in Fig. 14 indicates strong radiation losses ($\geq$200–300 dB/mm). This is confirmed in Fig. 15. Radiation losses for modes above the light line in a slab waveguide are expected to be proportional to the square of the vertical index contrast ($\Delta\varepsilon^2$) [9]. Thus, in III–V-based heterostructures intrinsic losses are much lower than in SOI-based waveguides. However, in silicon-based

structures some modes exist below the light line, with correspondingly very small intrinsic losses for guided modes. Only in the case of periodicity breaking, like waveguide bends, some intrinsic losses have to be expected below the light line, that depend on a complex way on several parameters such as dielectric contrast and defect design.

For the guided modes to become good candidates for waveguiding, some modifications of the defect design are necessary. Indeed, the extreme flatness of the band under the light line, in the case of the W1 waveguide discussed here, is in most cases not desirable because it leads to very low transmission. Furthermore, since in the region of guided modes the defect band is located very close to the lower edge of the band gap, it is expected to be not well confined and very sensitive to fabrication disorder. A way to shift the defect mode in the middle of the band gap, as well as to increase the group velocity and the transmission window of the mode below the light line, is to vary the defect width. The position of the mode within the band gap can be also controlled by varying the diameter of the holes constituting the line defect or of the holes surrounding the defect [31,45].

6. Conclusion

In summary, 2D photonic crystals offer the exciting possibility to guide light in two and three dimensions, by combining two different guiding mechanisms: index guiding and photonic-band-gap guiding. A line defect in the plane of the photonic crystal acts as a waveguide with bounded defect states. Some of these states exist already below the bulk modes and are guided by total internal reflection. They see the photonic crystal as a more or less homogeneous medium with effective refractive index. These modes are very similar to ridge waveguide modes. Some other modes are confined within the line defect due to destructive interferences with the surrounding photonic crystal. This second guiding mechanism is based only on the existence of the photonic band gap and do not exist in a ridge waveguide. If the photonic crystal is fabricated in a thin dielectric slab, light can also be confined in the vertical direction by total internal reflection due to the index contrast between the slab and its surrounding. Combined with the waveguiding along a line defect within the plane of the photonic crystal, a possible 3D light confinement in 2D photonic crystals can be achieved.

We appreciate funding by the BMBF within the project HiPhoCs. We are also grateful to M. Agio, J. Schilling, F. Müller, T. Geppert, and R. Hillebrand for stimulating discussions.

References

[1] S. John, Phys. Rev. Lett. 58 (1987) 23.
[2] E. Yablonovitch, Phys. Rev. Lett. 58 (1987) 20.
[3] J.D. Joannopoulos, R.D. Meade, J.N. Winn, Photonic Crystals, Molding the Flow of Light, Princeton Academic Press, Princeton, NJ, 1995.
[4] J. Schilling, F. Müller, et al., Appl. Phys. Lett. 78 (2001) 1180.
[5] A. Birner, R.B. Wehrspohn, et al., Adv. Mater. 13 (2001) 377.
[6] S. Noda, K. Tomoda, et al., Science 289 (2000) 604.
[7] A. Blanco, E. Chomski, et al., Nature 405 (2000) 437.
[8] S.Y. Lin, J.G. Fleming, et al., J. Opt. Soc. Am. B 18 (2001) 32.
[9] H. Benisty, D. Labilloy, et al., Appl. Phys. Lett. 76 (2000) 532.
[10] S.G. Johnson, S. Fan, et al., Phys. Rev. B 60 (1999) 5751.
[11] P.R. Villeneuve, S. Fan, et al., IEE Proc. Optoelectron. 145 (1998) 384.
[12] C. Weisbuch, H. Benisty, et al., Phys. Stat. Sol. 221 (2000) 93.
[13] M. Megens, J. Wijnhoven, et al., Phys. Rev. A 59 (1999) 4727.
[14] K. Busch, S. John, Phys. Rev. E 58 (1998) 3896.
[15] F. Genereux, S.W. Leonard, et al., Phys. Rev. B 63 (2001) 161101.
[16] H. Kosaka, T. Kawashima, et al., Phys. Rev. B 58 (1998) 10096.
[17] W. Park, C.J. Summers, Opt. Lett. 27 (2002) 1397.
[18] C. Luo, S.G. Johnson, et al., Phys. Rev. B 65 (2002) 201104.
[19] M. Notomi, Phys. Rev. B 62 (2000) 10696.
[20] R.D. Meade, K.D. Brommer, et al., Appl. Phys. Lett. 61 (1992) 495.
[21] S.G. Johnson, J.D. Joannopoulos, Opt. Express 8 (2001) 173.
[22] C. Jamois, R.B. Wehrspohn, et al., IEEE J. Quant. Electron. 38 (2002) 805.
[23] V. Lehmann, H. Föll, J. Electrochem. Soc. 137 (1990) 653.
[24] V. Lehmann, J. Electrochem. Soc. 140 (1993) 2836.
[25] J. Schilling, A. Birner, et al., Opt. Mater. 17 (2001) 7.
[26] J. Schilling, R.B. Wehrspohn, et al., J. Opt. A: Pore Appl. Opt. 3 (2001) 121.
[27] M. Lončar, T. Doll, et al., J. Lightwave Technol. 18 (2000) 1402.
[28] T. Baba, A. Motegi, et al., IEEE J. Quant. Electron. 38 (2002) 743.

[29] A. Talneau, L. Le Gouezigou, N. Bouadma, Opt. Lett. 26 (2001) 1259.
[30] C. Weisbuch, H. Benisty, et al., IEICE Trans. Commun. 84 (2001) 1286.
[31] M. Notomi, A. Shinya, et al., IEEE J. Quant. Electron. 38 (2002) 736.
[32] W. Bogaerts, V. Wiaux, et al., IEEE J. Selec. Top. Quant. Electron. 8 (2002) 928.
[33] W. Bogaerts, P. Bienstman, R. Baets, Opt. Lett. 28 (2003) 689.
[34] M. Qiu, Appl. Phys. Lett. 81 (2002) 1163.
[35] L.C. Andreani, M. Agio, IEEE J. Quant. Electron. 38 (2002) 891.
[36] M. Galli, M. Agio, et al., Eur. Phys. J. B 27 (2002) 79.
[37] T. Ochiai, K. Sakoda, Phys. Rev. B 63 (2001) 125107.
[38] M. Qiu, B. Jaskorzynska, et al., Micr. Opt. Technol. Lett. 34 (2002) 387.
[39] C.T. Chan, Q.L. Yu, K.M. Ho, Phys. Rev. B 51 (1995) 16635.
[40] S.G. Johnson, P. Villeneuve, et al., Phys. Rev. B 62 (2000) 8212.
[41] W.T. Lau, S. Fan, Appl. Phys. Lett. 81 (2002) 3915.
[42] S.W. Leonard, H.M. van Driel, et al., Opt. Lett. 25 (2000) 1550.
[43] L.C. Andreani, M. Agio, Appl. Phys. Lett. 82 (2003) 2011
[44] M. Lončar, D. Nedeljković, et al., Appl. Phys. Lett. 80 (2002) 1689.
[45] M. Lončar, J. Vučković, A. Scherer, J. Opt. Soc. Am. B 18 (2001) 1362.